INDIAN JOURNAL OF SCIENCE AND TECHNOLOGY

RESEARCH ARTICLE

Cerium Oxide Nanoparticle-Papain Enzyme Bioconjugate: Synthesis, Characterization and Optical Absorption Study for Biomedical Applications

Goutam Mandal[1,2]*, Baibaswata Bhattacharjee[3]

1 Department of Physics, Bankura Zilla Saradamani Mahila Mahavidyapith, Bankura, 722101, West Bengal, India
2 Department of Physics, Bankura University, Bankura, 722146, West Bengal, India
3 Department of Physics, Ramananda College, Bishnupur, Bankura, 722122, West Bengal, India

OPEN ACCESS

Received: 31-01-2024
Accepted: 07-03-2024
Published: 22-03-2024

Citation: Mandal G, Bhattacharjee B (2024) Cerium Oxide Nanoparticle-Papain Enzyme Bioconjugate: Synthesis, Characterization and Optical Absorption Study for Biomedical Applications. Indian Journal of Science and Technology 17(13): 1331-1339. https://doi.org/10.17485/IJST/v17i13.270

* **Corresponding author**.

phy.gmandal@gmail.com

Funding: None

Competing Interests: None

Published By Indian Society for Education and Environment (iSee)

ISSN
Print: 0974-6846
Electronic: 0974-5645

Abstract

Objective: Here, we synthesize cerium oxide nanoparticles, successfully characterize them, and study the interaction between enzymes and cerium oxide nanoparticles (CeO_2 NPs) using a simple optical spectroscopic technique. **Method:** CeO_2 was fabricated by chemical method. Characterizations were done using UV-Vis absorption spectra, FESEM images, and XRD data. For the biomolecular study, papain was used as a model enzyme. Two different concentrations of CeO_2, namely a small concentration range (0.05810 to 0.40670 mM) and a large concentration range (0.58100 to 0.92961 mM), were taken to study the interaction with the papain. UV-Vis absorption spectra were recorded to study bioconjugate formation. **Findings:** The CeO_2 NPs have an intense absorption peak at 352 nm and a band gap of 3.78 eV. The XRD pattern showed the unit cell is cubic with an average particle size of 41.36 nm. The binding of papain with CeO_2 NPs resulted in a red shift in its absorption peak. The apparent association constant (Kapp) was calculated for the bioconjugate and found to be 0.747×10^3 M^{-1} for small concentrations and 0.278×10^3 M^{-1} for large concentrations. In large concentrations, aggregation occurs instead of corona formation. **Novelty:** To the best of our knowledge, this may be the first study of the interaction of papain enzyme with CeO_2 NPs. This study contributes to the application of NPs in the field of biomedicine.

Keywords: Cerium oxide; Papaya proteinase (PP); Absorption spectra; Bioconjugate; Association constant

1 Introduction

Nanotechnology attracts much attention for its fundamental studies and potential applications in the biomedical field and drug delivery processes [(1)]. The biocompatibility of nanomaterials depends on their physical and chemical properties. Upon entering the

biological system, nanomaterials interact with a broad range of soluble biomolecules. Adsorbed Interaction between NPs and biomolecules produces a biomolecular corona[2]. This biomolecular corona alters the nanoparticles' size, surface charge, and composition and gives them a biological identity that is different from the original[3]. The components of a biological system perceive the biological identity. Biomolecule-nanoparticle interactions modify a nanoparticle's aggregation state, activity, and dissolution properties[4].

Papaya latex (*Carica papaya* L.) contains papain, a plant cysteine protease enzyme. To extract papain, one slices the skin of an unripe papaya and collects and dries the latex that drains from the wound. The papain enzyme belongs to the papain superfamily of proteolytic enzymes. As a proteolytic enzyme, it is essential for several critical biological processes in every living organism[5]. The papain has a wide proteolytic action against proteins, amino acid esters, short-chain peptides, and amide bonds and is extensively used in food and medicine. It preferentially degrades peptide bonds that include basic amino acids, including arginine, lysine, and residues immediately after phenylalanine[6]. Papain's unique structure facilitates the understanding of its proteolytic enzyme activity and its potential applications.

On the other hand, the cerium oxide (CeO_2) nanoparticle is a direct and large band gap ($E_g = 3.19\ eV$) semiconductor[7]. Nanoceria have attracted considerable interest because to their widespread use in environmental remediation, photocatalytic dye degradation, biological applications, and industrial sectors[8]. Because of their higher exciton binding energy, they are an excellent contender for catalytic applications. The catalytic antioxidant characteristics of CeO_2 NPs can be used for treatment of oxidative stress diseases[9]. CeO_2 NP surfaces show biological activity. The Ce^{3+} /Ce^{4+} redox pair pathway of CeO_2 provides antioxidant and antiradical activities. Nanoceria exhibit a variety of roles in the cellular and tissue buffering of reactive oxygen species (ROS)[10]. CeO_2 NPs resemble the function of superoxide dismutase (SOD) and are used to treat oxidative stress-related illnesses like endometriosis[11], anti-angiogenic[12] neurodegeneration[13], chronic inflammation[14], diabetes[15], retinitis[16] and cancer[17]. Thus, it is particularly important to investigate the interactions of CeO_2 NPs in various biological media in order to investigate their medicinal applicability in plasma and other biological mediums. In order to improve research and use of CeO_2 NPs in biomedicine[18], it is necessary to study how they interact with biomolecules and biofluids found in the human body. Although cerium oxide nanoparticles have made significant progress in biomedical applications, they still face physicochemical challenges such as loss of enzymatic activity during storage, non-specific cellular uptake, and off-target toxicities[19]. To explore the biological applications of cerium oxide nanoparticles, studying the interaction between enzymes and cerium oxide is critical.

Considering this, the present work studied the interaction of the enzyme with CeO_2 using papain as a model enzyme. To the best of our knowledge, this is the first report on papain and CeO_2 NP bioconjugate. This study may aid in the understanding of the corona formation of enzymes with nanomaterials and can be applied in the biomedical field.

2 Methodology

2.1 Materials

Cerium nitrate hexahydrate and potassium carbonate were obtained from Sigma-Aldrich. The reagents were used without further purification. The papaya milk was collected from papaya fruit and mixed with deionized water for the bioconjugate experiment.

2.2 Collection of papaya proteinase

Papain that is found in papaya fruit was collected from the local area of the district of Bankura (23.1645° N, 87.0624° E), West Bengal, India. The fruit was properly rinsed under tap water before being cleansed with distilled water. The chemical structure and properties of papain are shown in Table 1.

Table 1. Properties of papain

Material	DNA structure	λ_{max}(nm)	MW(g/mol)	Molecular formula
Papain	Figure 1	275	226.23	$C_9H_{14}N_4O_3$

2.3 Synthesis CeO_2 nanoparticles

A novel method was used to synthesise CeO_2 nanoparticles, as described below. We prepared a 0.03M solution by mixing 3.257 g of $Ce(NO_3)_3$.$6H_2O$ in 250 mL of deionized water. Similarly, a 0.03M solution of potassium carbonate [K_2CO_3] was prepared by mixing 1.036 g of K_2CO_3 in 250 mL of deionized water. While maintaining a pH of 9, we added 50 mL of cerium

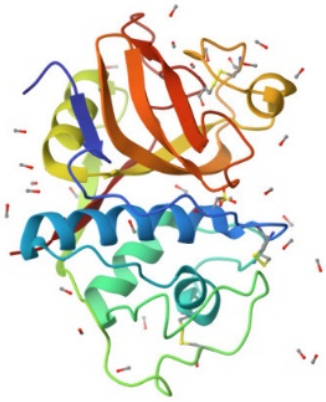

Fig 1. DNA structure

nitrate solution and 30 mL of potassium carbonate drop by drop to 100 mL of well-stirred water under a magnetic stirrer. After continuing magnetic stirring for the next 3 hours at room temperature, we obtained a precipitate of cerium (III) carbonate. We separated the precipitate on filter paper and rinsed it with deionized water multiple times. The precipitate was dried in a hot air oven at 60° C for 3 hours, then calcined at 600° C for 6 hours. The synthesis process is shown in Figure 2.

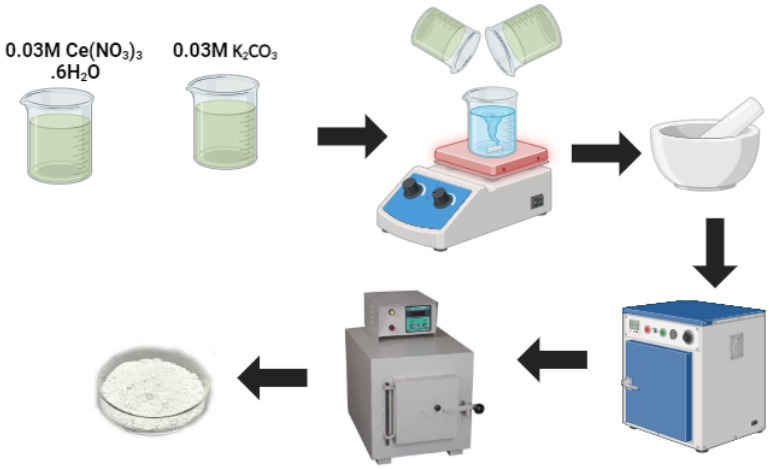

Fig 2. Schematic synthesis process of CeO_2 NPs

2.4 Characterization techniques

A Systronics (AU 2703) double-beam UV-Vis spectrophotometer was used to take the optical absorption data. A ZEISS field emission scanning electron microscope (FESEM) at an operating voltage of 5 kV was used to study the surface morphology. A Rigaku X-ray diffractometer was used to study the crystallinity by employing Cu-Kα radiation at a wavelength of 1.54 A^0 in the angular range of 20^0 to 80^0.

2.5 Bioconjugate experiment

The papain (PP) solutions with a preset concentration were prepared using one drop of papaya milk in 100 ml ($C_{PP} = 1drop/100\ ml$) triple distilled water. The freshly prepared water has a pH of 6.8 and resistivity of 18.2 Ω cm. Ultrasonication was used to disperse the ready CeO_2 NPs in water for 60 minutes. The concentration of the CeO_2 solution changes as required by adding triple distilled water. The mixed solution of CeO_2 NPs and papain were prepared through mixing preset aqueous papain solution with the CeO_2, ranging from 0.05810 mM to 0.92961 mM with proper ratio.

3 Result and discussion

3.1 Optical properties

The optical band gap of the nanocrystal was calculated by examining its optical properties using a UV-Vis spectrophotometer in the wavelength range of 200 nm to 800 nm. (Figure 3 **(A)**). The strongest absorbance peak was observed at around 352 nm. In the wavelength range 200-800 nm, the absorption coefficient (α) was computed by using the Lambert law. To determine the excitonic band gap (E_g) of the CeO_2 nanoparticles, the Tauc equation [20] was used, as shown below.

$$(\alpha h\nu)^2 = B(h\upsilon - E_g)$$

Where $\alpha = 2.303\frac{A}{t}$ (A is absorbance), h is known as Planck's constant, υ is frequency and B is band tailing parameter. The plot of $h\upsilon$ vs. $(\alpha h\upsilon)^2$ is shown in Figure 3**(B)**, which is used to find the band gap E_g by extrapolating the linear part on the abscissa. The calculated direct excitonic band gap was 3.78 eV.

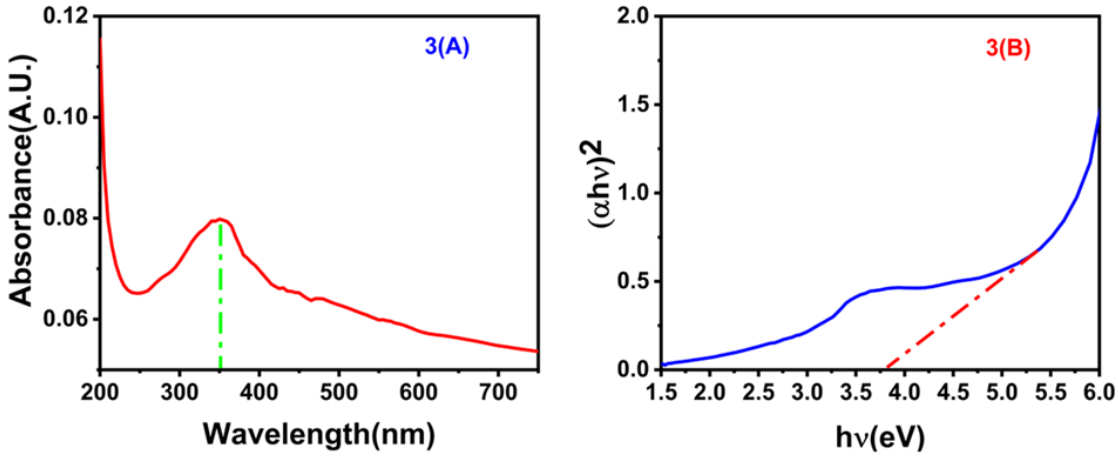

Fig 3. (A) UV-VIS spectrum of CeO_2 NPs, (B) Tauc's plot for band gap determination

3.2 Structural analysis

3.2.1 FE SEM

SEM analysis was used to study the surface morphology of CeO_2 nanoparticles. The surface morphology is given in Figure 4. The image demonstrates that flower-like nanoparticles were produced. Also, there is a good separation of flower-like structures. The possible reason for such formation was due to ageing effect.

3.2.2 X-Ray diffraction

Figure 5 **(A)** depicts the powder XRD pattern of the synthesised CeO_2 nanocrystal, with diffraction peaks at (111), (200), (220), (311), (222), (400), (331) and (420). The peaks can be well indexed with the face-centred cubic fluorite structure of nanoceria (JCPDS 96-900-9009). The nanocrystal exhibits a maximum peak intensity at $2\theta = 28.6202\ A^0$ associated with (111) Miller

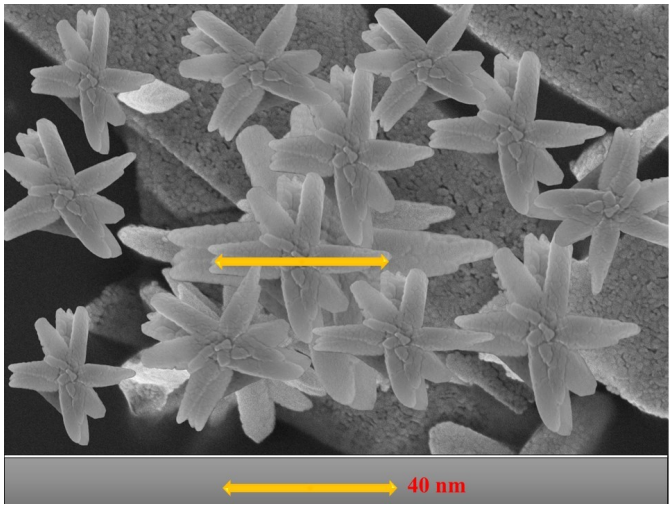

Fig 4. FESEM image of CeO_2 nano-flower with scale 40 nm

planes, which was used to estimate the crystallographic parameters. The size of the nanocrystal (D_V) was computed by Debye-Scherer formula[21]

$$D_V = \frac{K\lambda}{\beta_{1/2} cos\theta}$$

Here, K = 0.94, for copper radiation.

Figure 5**(B)** illustrates the variation of FWHM or half width ($\beta_{1/2}$) according to distinct diffraction peaks at 2θ.

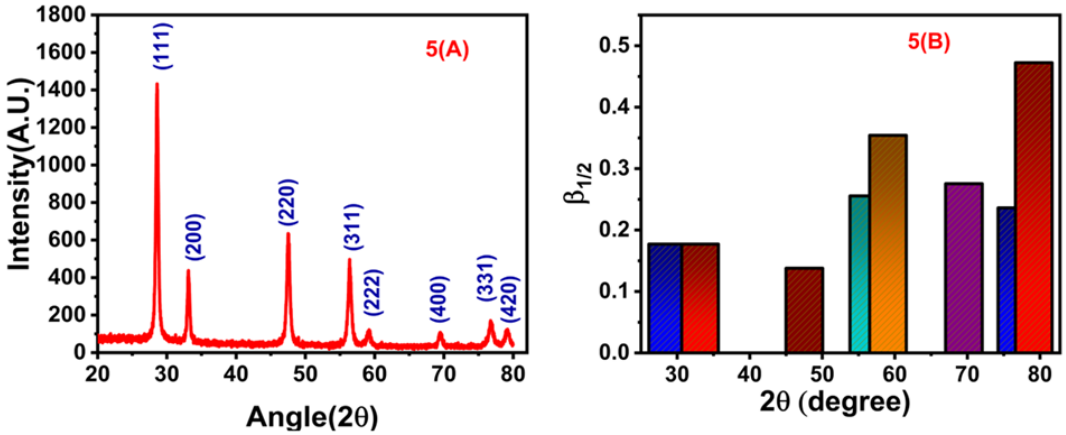

Fig 5. (A)XRD pattern of the CeO_2 nano-crystal (B) variation of half width ($\beta_{1/2}$) of the different diffraction peaks with peak position (2θ)

The dislocation density (δ_D), and the microstrain (ε_m) of the nanocrystal are determined according to the following equations:

$$\delta_D = \frac{1}{D_V^2}$$

$$\varepsilon_m = \frac{\beta_{1/2} cos\theta}{4}$$

The crystallite size and microstrain was also calculated using Williamson–Hall (W-H) equation

$$\beta_{1/2} cos\theta = \frac{K\lambda}{D_V} + 4\varepsilon_m sin\theta$$

The linear fit of W-H plot gives the value of microstrain (ε_m) and crystallite size (D_V). Slope of the graph gives microstrain and intercept on y axis gives the crystallite size.

The CeO_2 nanocrystal's lattice constant (a) was determined using the following equation:

$$a = \sqrt{3} \times d_{111}$$

Here, d_{111} is the interplanar spacing of (111) planes. Different lattice parameters of the nano sample are listed in Table 2.

Table 2. Different crystal parameters

(hkl) plane	d spacing(A^0)	Lattice constant a	Scherrer's method			Williamson–Hall method		
			Grain size (D_V)	Microstrain (ε_m)	Dislocation density (δ_D)	Grain size (D_V)	Microstrain (ε_m)	Dislocation density (δ_D)
(111)	3.119	5.4022	48.3272	0.000748	0.000428	41.3466	0.000968	0.000796

3.3 Concentration dependent absorption spectrum of CeO_2 -papain bioconjugates

To investigate the specific molecular interaction between CeO_2 NPs and papain (PP), the absorption spectra of papain were monitored in the absence and presence of CeO_2. Figure 6 shows the UV-Vis absorption spectrum of pure papain (without CeO_2 NPs) at a preset concentration. A strong absorption peak at 275 nm was observed.

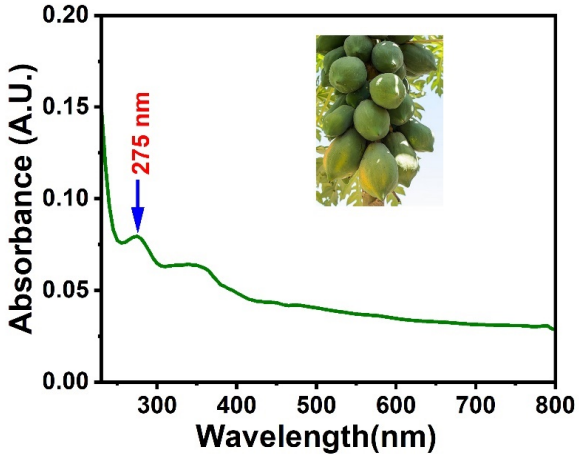

Fig 6. UV absorption spectra of papain biomolecule with papaya is inset

To determine the molecular interaction between CeO_2 NP and papain, the absorption spectra of papain were measured in the absence and presence of CeO_2 NPs. Two different ranges of concentrations of CeO_2 nanoparticles were taken to investigate the biomolecular interactions of the nanoparticles with papain. The concentration range from 0.05810 mM to 0.40670 mM was referred to as the small concentration range, and from 0.58100 mM to 0.92961 mM was referred to as the large concentration range.

Figure 7**(A)** shows the absorption spectra of papain and CeO_2 NPs–Papain bioconjugatein the small concentration range. The absorbance peak (at 275 nm) of papain increased when the concentration of CeO_2 NPs within the CeO_2-PP bioconjugate increased. With the addition of CeO_2 NPs in this range, the absorption peak of free papain (PP) (~ 275 nm) broadens. The shape of the peak at ~ 275 nm for free PP changes when CeO_2 nanoparticles are added to the bioconjugate. Within the bioconjugate,

the maximum absorbance peak (~ 352 nm) for CeO_2 nanoparticles also increases. The formation of the ground state complex enhances the overall absorbance of the CeO_2 NPs-papain system.

The introduction of a high quantity of CeO_2 NPs (Figure 7**(B)**) reduced the enzyme absorbance peak at 275 nm and considerably increased the peak of CeO_2 NPs. The large amount of doses reduces the peak of the papain enzyme at 275 nm. This might be owing to the higher concentration of CeO_2 NPs, which results in fewer papain molecules on the surface. Using small and large concentrations of CeO_2 NPs, we see a maximum redshift of ~10 nm and ~5 nm of papain absorbance, respectively. Also, the red shifting of the peak of papain biomolecule is an indication of formation of bioconjugate. As some part of the energy was used to form the bioconjugate therefore the absorption peaks shift to the lower energy. The red shift of the papain enzyme peak was caused by the transfer of energy between CeO_2 NPs and papain biomolecules.

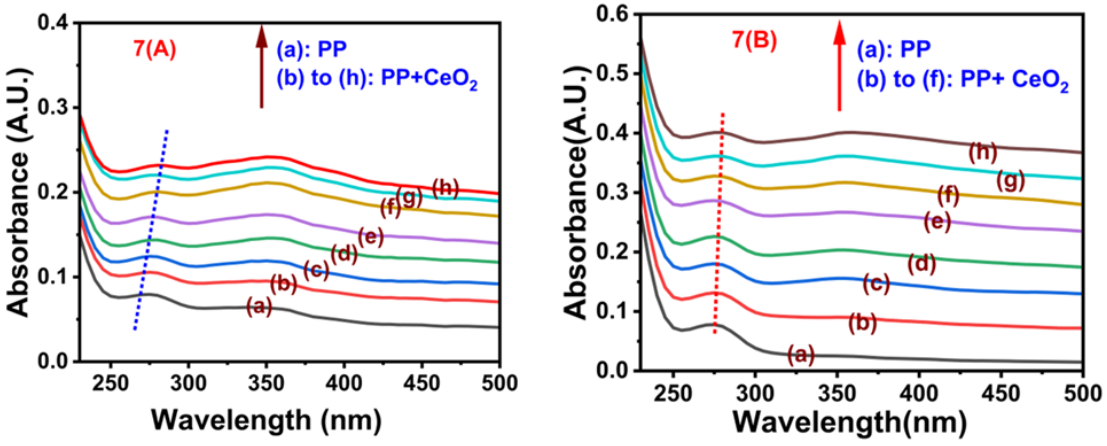

Fig 7. (A) Absorption spectra of (a) papain (PP) (b) CeO_2 0.05810 mM + PP (c) CeO_2 0.11620 mM + PP (d) CeO_2 0.17430 mM + PP (e) CeO_2 0.23240 mM + PP (f) CeO_2 0.29050 mM + PP (g) CeO_2 0.34860 mM + PP (h) CeO_2 0.40670 mM + PP, (B) Absorption spectra of (a) papain (PP) (b) CeO_2 0.58100 mM + PP (c) CeO_2 0.63910 mM + PP (d) CeO_2 0.69720 mM + PP (e) CeO_2 0.75530 mM + PP (f) CeO_2 0.81340 mM + PP (g) CeO_2 0.87150 mM + PP (h) CeO_2 0.92961 mM + PP

To quantitatively compare the binding strength of CeO_2 NPs, the apparent association constants or binding constant (K_B) with PP were determined by monitoring changes in PP absorbance at 275 nm.

The equilibrium for CeO_2 NPs-PP complex bioconjugate production is described by:

$PP + CeO_2 \rightarrow K_B \rightarrow CeO_2 : PP$ complex.

The binding constant (K_B) of a complex can be expressed as the concentration of components at equilibrium.

$$K_B = \frac{[CeO_2 : PP]}{[CeO_2]\,[PP]}$$

The Benesi and Hildebrand method was used to compute the value of the association constant (K_B) [22]:

$$\frac{1}{A_c - A_0} = \frac{1}{A_{max} - A_o} + \frac{1}{K_B\,(A_{max} - A_0)}\,\frac{1}{[Q]}$$

Here [Q] is the concentration of CeO_2, A_0 is the absorbance of papain in absence of CeO_2 (initial absorbance), A_c is the recorded absorbance at 275 nm of papain at different CeO_2 concentration c and A_{max} is the maximum absorbance.

The variation of $\frac{1}{A_c - A_0}$ versus 1/[Q] corresponding to the small concentration and large concentration ranges are shown in Figure 8**(A)** and **(B)** respectively. In Figure 8 **(A)**, the plot of $\frac{1}{A_c - A_0}$ vs. 1/[Q] shows a straight line, demonstrating a 1:1 complexation between CeO_2 and PP. From the linear fittings of the data, the slope gives the value of $\frac{1}{K_B(A_{max} - A_0)}$ and intercept gives the value of $\frac{1}{A_{max} - A_o}$. The value of K_B was estimated to be 0.747×10^3 M^{-1} (R=0.9952, where R is correlation coefficient) for small concentration range and 0.278×10^3 M^{-1} (R=0.9188) for the large concentration range. The higher value of apparent association constant K_B in the low concentration zone supports a large number of enzymes on the CeO_2 NPs surfaces. Thus, a strong enzyme-CeO_2 NPs complex formed in the ground state in compare with the high concentration region.

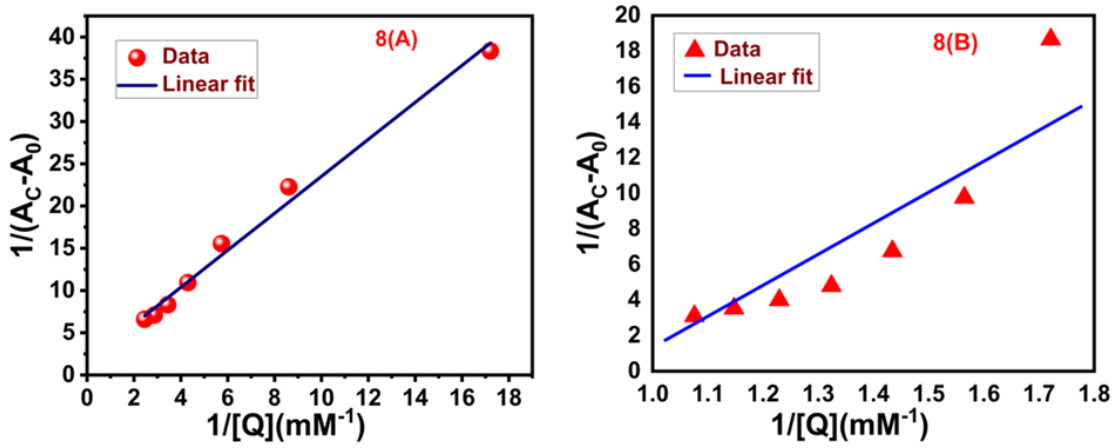

Fig 8. (A) Plot of $\frac{1}{A_c - A_0}$ versus 1/Q in the small concentration range, (B) Plot of $\frac{1}{A_c - A_0}$ versus 1/Q in the large concentration range

The schematic representation of bioconjugate formation at different concentrations of CeO_2 is shown in Figure 9.

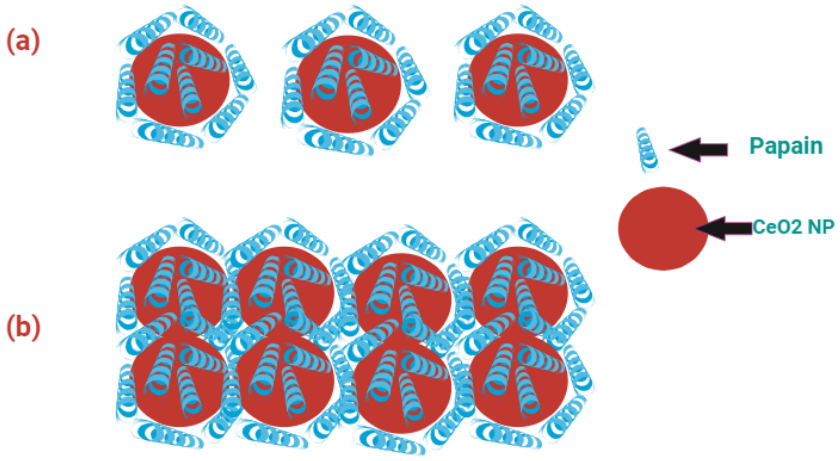

Fig 9. Schematic representation of corona formation between papain and different-concentration CeO_2 nanoparticles: (a) small concentration of CeO_2 NPs, (b) large concentration of the CeO_2 NPs

4 Conclusion

In conclusion, we successfully grew CeO_2 NPs using the low-cost chemical precipitation approach and investigated their optical and structural characteristics. The nano biomolecular interactions were studied by simple absorption spectroscopy. The peak of the papain at 275 nm was red shifted due to nano-bio interactions. In our work, shifting was 10 nm and 5 nm for papain absorbance, corresponding to the usage of CeO_2 NPs with small and large concentration ranges, respectively. The apparent association constant we found was 0.747×10^3 M^{-1} in small concentration and 0.278×10^3 M^{-1} in large concentration respectively. We notice that the lower concentration of CeO_2 NPs results in a greater number of papain molecules per particle surface. Whereas a high concentration of CeO_2 NPs results in just a few of papain molecules per particle surface. Thus, papain can form corona with CeO_2 NPs, which may affect their enzymatic activity. Further study might have implications for their

future use in biomedical applications.

Acknowledgement

Authors are thankful to the Department of Physics, Bankura University and Bankura Zilla Saradamani Mahila Mahavidyapith.

References

1) Kallur M, Chandraprabha MN, Rajan HK, Khosla A, Manjunatha C. Synthesis, Characterization of Cerium Oxide Nanoparticles and Evaluation of DNA Binding Interactions. *ECS Transactions*. 2022;107(1):15935–15943. Available from: https;//doi.org/10.1149/10701.15935ecst.
2) Nienhaus K, Wang H, Nienhaus GU. Nanoparticles for biomedical applications: exploring and exploiting molecular interactions at the nano-bio interface. *Materials Today Advances*. 2020;5:1–20. Available from: https://doi.org/10.1016/j.mtadv.2019.100036.
3) Bilardo R, Traldi F, Vdovchenko A, Resmini M. Influence of surface chemistry and morphology of nanoparticles on protein corona formation. *WIREs Nanomedicine and Nanobiotechnology*. 2022;14(4):1–22. Available from: https://doi.org/10.1002/wnan.1788.
4) Tumkur PP, Gunasekaran NK, Lamani BR, Bayon NN, Prabhakaran K, Hall JC, et al. Cerium Oxide Nanoparticles: Synthesis and Characterization for Biosafe Applications. *Nanomanufacturing*. 2021;1(3):176–189. Available from: https://doi.org/10.3390/nanomanufacturing1030013.
5) Tacias-Pascacio VG, Morellon-Sterling R, Castañeda-Valbuena D, Ángel Berenguer-Murcia, Kamli MR, Tavano O, et al. Immobilization of papain: A review. *International Journal of Biological Macromolecules*. 2021;188:94–113. Available from: https://doi.org/10.1016/j.ijbiomac.2021.08.016.
6) Morellon-Sterling R, Tavano O, Bolivar JM, Ángel Berenguer-Murcia, Vela-Gutiérrez G, Sabir JSM, et al. A review on the immobilization of pepsin: A Lys-poor enzyme that is unstable at alkaline pH values. *International Journal of Biological Macromolecules*. 2022;210:1–21. Available from: https://doi.org/10.1016/j.ijbiomac.2022.04.224.
7) Pansambal S, Oza R, Borgave S, Chauhan A, Bardapurkar P, Vyas S, et al. Bioengineered cerium oxide (CeO2) nanoparticles and their diverse applications: a review. *Applied Nanoscience*. 2023;13(9):6067–6092. Available from: https://doi.org/10.1007/s13204-022-02574-8.
8) Singh KR, Vanya Nayak, Sarkar T, Singh RP. Cerium oxide nanoparticles: properties, biosynthesis and biomedical application. *RSC Advances*. 2020;10(45):27194–27214. Available from: https://doi.org/10.1039/D0RA04736H.
9) Kim YG, Lee Y, Lee N, Soh M, Kim D, Hyeon T. Ceria-Based Therapeutic Antioxidants for Biomedical Applications. *Advanced Materials*. 2024;36(10). Available from: https://doi.org/10.1002/adma.202210819.
10) Yadav N, Patel V, Mccourt L, Ruppert M, Miller M, Inerbaev T, et al. Tuning the enzyme-like activities of cerium oxide nanoparticles using a triethyl phosphite ligand. *Biomaterials Science*. 2022;10(12):3245–3258. Available from: https://doi.org/10.1039/D2BM00396A.
11) Biram DM, Hussein Y, Salem RR. Toxic Effect of Subchronic Use of Arsenic on the Liver of Adult Male Albino Rats and the Ameliorating Effect of Cerium Oxide Nanoparticles: Biochemical and Histological Study. *Egyptian Journal of Histology*. 2023;46(2):743–753. Available from: https://dx.doi.org/10.21608/ejh.2022.109555.1600.
12) Yong JM, Fu L, Tang F, Yu P, Kuchel RP, Whitelock JM, et al. ROS-Mediated Anti-Angiogenic Activity of Cerium Oxide Nanoparticles in Melanoma Cells. *ACS Biomaterials Science & Engineering*. 2022;8(2):512–525. Available from: https://doi.org/10.1021/acsbiomaterials.1c01268.
13) Yadav N, Singh S. SOD mimetic cerium oxide nanorods protect human hepatocytes from oxidative stress. *Emergent Materials*. 2021;4(5):1305–1317. Available from: https://doi.org/10.1007/s42247-021-00220-7.
14) Zou H, Wang H, Xu B, Liang L, Shen L, Lin Q. Regenerative cerium oxide nanozymes alleviate oxidative stress for efficient dry eye disease treatment. *Regenerative Biomaterials*. 2022;9:1–13. Available from: https://doi.org/10.1093/rb/rbac070.
15) Casals G, Perramón M, Casals E, Portolés I, Fernández-Varo G, Morales-Ruiz M, et al. Cerium Oxide Nanoparticles: A New Therapeutic Tool in Liver Diseases. *Antioxidants*. 2021;10(5):1–23. Available from: https://doi.org/10.3390/antiox10050660.
16) Badia A, Duarri A, Salas A, Rosell J, Ramis J, Gusta MF, et al. Repeated Topical Administration of 3 nm Cerium Oxide Nanoparticles Reverts Disease Atrophic Phenotype and Arrests Neovascular Degeneration in AMD Mouse Models. *ACS Nano*. 2023;17(2):910–926. Available from: https://doi.org/10.1021/acsnano.2c05447.
17) Cheng G, Guo W, Han L, Chen E, Kong L, Wang L, et al. Cerium oxide nanoparticles induce cytotoxicity in human hepatoma SMMC-7721 cells via oxidative stress and the activation of MAPK signaling pathways. *Toxicology in Vitro*. 2013;27(3):1082–1088. Available from: https://doi.org/10.1016/j.tiv.2013.02.005.
18) Pesaraklou A, Matin MM. Cerium oxide nanoparticles and their importance in cell signaling pathways for predicting cellular behavior. *Nanomedicine*. 2020;15(17):1709–1718. Available from: https://doi.org/10.2217/nnm-2020-0104.
19) Wang M, He H, Liu D, Ma M, Zhang Y. Preparation, Characterization and Multiple Biological Properties of Peptide-Modified Cerium Oxide Nanoparticles. *Biomolecules*. 2022;12(9):1–16. Available from: https://doi.org/10.3390/biom12091277.
20) Coulter JB, III DPB. Assessing Tauc Plot Slope Quantification: ZnO Thin Films as a Model System. *physica status solidi (b)*. 2018;255(3). Available from: https://doi.org/10.1002/pssb.201700393.
21) Mustapha S, Ndamitso MM, Abdulkareem AS, Tijani JO, Shuaib DT, Mohammed AK, et al. Comparative study of crystallite size using Williamson-Hall and Debye-Scherrer plots for ZnO nanoparticles. *Advances in Natural Sciences: Nanoscience and Nanotechnology*. 2019;10(4). Available from: https://iopscience.iop.org/article/10.1088/2043-6254/ab52f7.
22) Akram D, Elhaty IA, Alneyadi SS. Synthesis and Antibacterial Activity of Rhodanine-Based Azo Dyes and Their Use as Spectrophotometric Chemosensor for Fe3+ Ions. *Chemosensors*. 2020;8(1):1–13. Available from: https://doi.org/10.3390/chemosensors8010016.